ELECTRONIC SUPPLEMENTARY INFORMATION

Polyoxometalates as advanced-performance anions for ~D_{5h} Dy(III) single-ion magnets

Ethan Lowe,[a] Claire Wilson,[a] Angelos B. Canaj*[a] and Mark Murrie*[a]

School of Chemistry, University of Glasgow, University Avenue, Glasgow, G12 8QQ, UK.
E-mail: tsanai.angelos@gmail.com , mark.murrie@glasgow.ac.uk.

Abstract We enhance single-ion magnet (SIM) magnetisation reversal barriers by engineering the second coordination sphere, substituting conventional small monoanions with a bulky polyoxometalate (POM) trianion. Importantly, our approach serves as a model for creating new high-performance multifunctional hybrid materials.

Experimental Methods

All experiments were carried under aerobic conditions using materials and solvents as received without further purification. Elemental analyses (C, H, N) were performed by the University of Glasgow microanalysis service. Powder X-ray diffraction data were collected on freshly prepared samples of $[Dy(H_2O)_5(Cy_3PO)_2][W_{12}PO_{40}]\cdot 2(Cy_3PO)\cdot 5THF\cdot H_2O$ (**1**) on a Rigaku MiniFlex benchtop diffractometer equipped with a Cu sealed tube X-ray source (λ (CuKα) = 1.5405 Å) and a 6-position sample changer on zero-background silicon sample holders at the University of Glasgow. Single Crystal X-Ray diffraction data were collected at the EPSRC National Crystallographic Service at the University of Southampton (see .cif for details).

Variable-temperature, solid-state direct current (dc) magnetic susceptibility data were collected on a Quantum Design MPMS3 SQUID magnetometer at the University of Glasgow and on a Quantum Design Dynacool PPMS equipped with a 9 T magnet at the University of Edinburgh. Ac magnetic susceptibility data were collected on a Quantum Design MPMS3 SQUID magnetometer at the University of Glasgow. Microcrystalline samples were prepared using a mortar and pestle in open air and then added to gelatin capsules in the presence of eicosane. Diamagnetic corrections were applied to the observed paramagnetic susceptibilities using Pascal's constants. The diamagnetic contribution of the sample holder and eicosane were corrected by measurements.

Synthesis and Characterisation

All reagents were used as received without further purification. No safety hazards were encountered during the described experimental procedures.

*Synthesis of $[Dy(H_2O)_5(Cy_3PO)_2](CF_3SO_3)_3\cdot 2(Cy_3PO)$ (**P1**)*

$Dy(CF_3SO_3)_3$ (0.6 mmol, 378mg) and Cy_3PO (2.4 mmol, 710 mg) were dissolved in 20 mL ethanol and heated at 70 °C for 5 hours. The resulting solution was filtered and layered with Et_2O at room temperature giving colourless crystals within hours, with a yield of 60%. Elemental analysis calculated % for $C_{75}H_{142}DyF_9O_{18}P_4S_3$: C, 47.77 %; H, 7.59 %; N, 0 %. Found: C, 47.40 %; H, 7.49 %; N, 0 %.

*Synthesis of $[Dy(H_2O)_5(Cy_3PO)_2][W_{12}O_{40}]\cdot 2(Cy_3PO)\cdot 5THF\cdot H_2O$ (**1**)*

(**P1**) (0.1 mmol, 189 mg) was dissolved in 5 mL of hot THF and $H_3[PW_{12}O_{40}]\cdot 24H_2O$ (0.1 mmol, 331 mg) was dissolved in 5 drops of deionised water. The solutions were combined giving a large amount of white precipitate and the mixture was heated at 60 °C for 1 hour. The precipitate was removed by filtration and colourless block crystals suitable for single crystal X-ray diffraction were obtained after 1-2 days, by slowly diffusing cold Et_2O into the solution. Yield ~50%. Elemental analysis calculated % for $C_{76}H_{152}DyP_5O_{51}W_{12}$ (**1** – 4THF): C, 20.72 %; H, 3.48 %; N: 0 %. Found: C, 20.74 %; H, 3.48 %; N: 0 %. Selected IR data: $\bar{\nu}$ (cm^{-1}) 803, 890, 977, 1076, 1237, 1448, 2365, 2852, 2925.

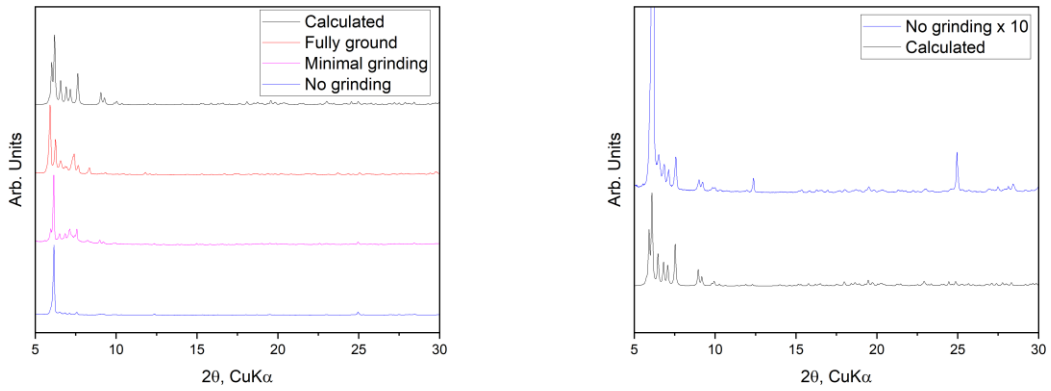

Figure S1 The powder X-ray diffraction pattern of **1** (left), where the black line represents the calculated X-ray diffraction pattern from a single crystal collected at 100 K; the red line represents the *fully ground* crystalline powder sample collected at room temperature; the pink line represents *minimal grinding* and the blue line indicates *no grinding* of the sample. The powder X-ray diffraction pattern of the unground sample of **1** (right) multiplied by ten, where the presence of higher intensity peaks at 6.16, 12.4 and 24.96° are attributed to the preferred orientation of the unground sample.

Table S1 Crystal Data and Structure Refinement Parameters for $[Dy(H_2O)_5(Cy_3PO)_2][W_{12}PO_{40}]\cdot 2(Cy_3PO)\cdot 5THF\cdot H_2O$ (**1**).

Empirical formula	$C_{92}H_{183}DyO_{55}P_5W_{12}$
Formula weight	4692.92
Temperature/K	100.15
Crystal system	triclinic
Space group	P-1
a/Å	14.8908(2)
b/Å	15.5061(2)
c/Å	28.8135(4)
α/°	102.0650(10)
β/°	91.0860(10)
γ/°	99.2480(10)
Volume/Å^3	6411.94(15)
Z	2
ρ_{calc}g/cm^3	2.431
μ/mm^{-1}	11.435
F(000)	4408.0
Crystal size/mm^3	0.04 × 0.04 × 0.02
Radiation	MoKα (λ = 0.71073)
2Θ range for data collection/°	3.2 to 52.744
Index ranges	-18 ≤ h ≤ 18, -19 ≤ k ≤ 19, -36 ≤ l ≤ 36
Reflections collected	84219
Independent reflections	26039 [R_{int} = 0.0723, R_{sigma} = 0.0668]
Data/restraints/parameters	26039/244/1524
Goodness-of-fit on F^2	1.020
Final R indexes [I>=2σ (I)]	R_1 = 0.0704, wR_2 = 0.1819
Final R indexes [all data]	R_1 = 0.0925, wR_2 = 0.1934
Largest diff. peak/hole / e Å^{-3}	3.01/-1.61

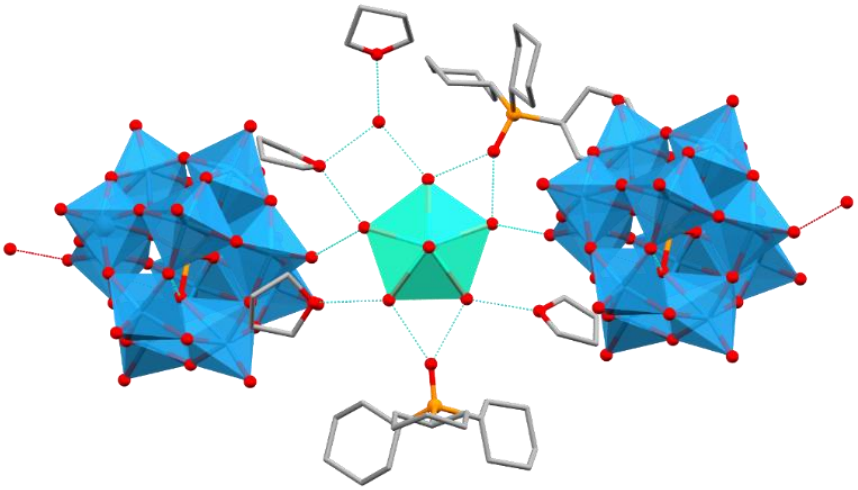

Figure S2 The hydrogen-bonding network in **1** with axial {Cy_3P} units and H atoms omitted for clarity. C, grey; Dy, cyan; O, red; P, orange; W, blue.

Table S2 A comparison of the hydrogen bonding between the oxygen donor (O_{eq}) of the equatorial H_2O molecules of $[Dy(H_2O)_5(Cy_3PO)_2]^{3+}$ and the second coordination sphere (HBA_{total} = all hydrogen bond acceptor molecules in the second coordination sphere).

Compound	Average $O_{eq}\cdots$Anion distance (Å)	Average $O_{eq}\cdots HBA_{total}$ (Å)	U_{eff} (K)	$T_{B(Hyst)}$ (K) (200 Oe/s)
$[Dy(Cy_3PO)_2(H_2O)_5]Cl_3\cdot(Cy_3PO)\cdot H_2O\cdot EtOH$ **C1**	3.16	3.00	472(7)	11
$[Dy(Cy_3PO)_2(H_2O)_5]Br_3\cdot 2(Cy_3PO)\cdot 2H_2O\cdot 2EtOH$ **C2**	3.22	2.99	543(2)	20
$[Dy(H_2O)_5(Cy_3PO)_2](CF_3SO_3)_3\cdot 2(Cy_3PO)$ **P1**	2.76	2.71	562(7)	n/a
1 This work	2.76	2.71	625(1)	12

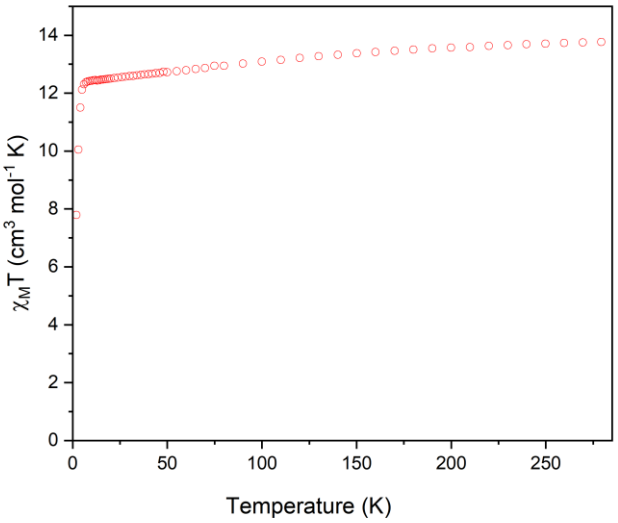

Figure S3 Molar magnetic susceptibility ($\chi_M T$) *vs.* Temperature for **1** at 1000 Oe from 280 – 2 K.

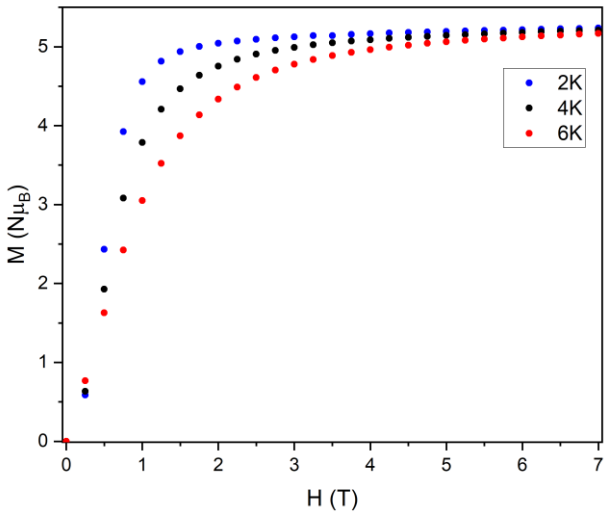

Figure S4 Magnetisation *vs.* Field plots for **1** at 2, 4 and 6 K.

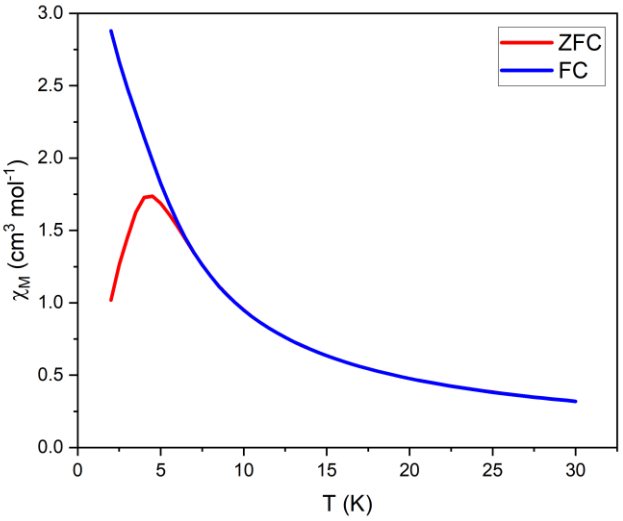

Figure S5 The field cooled (FC) and zero field cooled (ZFC) magnetic susceptibility of **1** at 1000 Oe, with a sweep rate of 2 K/min, diverging at 8 K, with a maximum at 4.5 K.

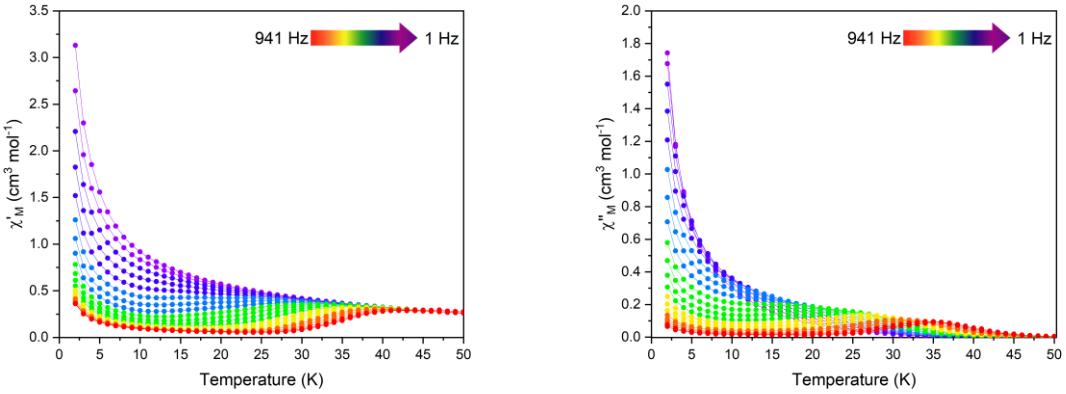

Figure S6 Temperature dependence of the in-phase (χ′M) (left) and out-of-phase(χ′′M) (right) magnetic susceptibility, under zero dc field, for **1.**

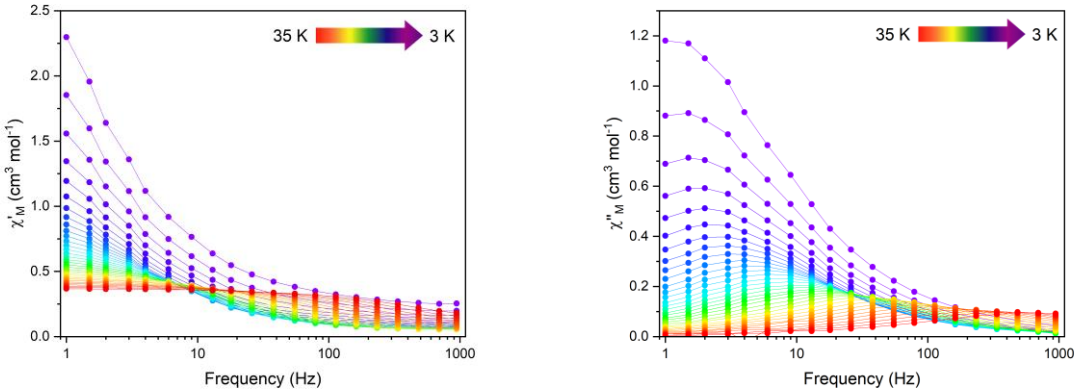

Figure S7 Frequency dependence of the in-phase (χ′M) (left) and out-of-phase (χ′′M) (right) magnetic susceptibility, under zero dc field, for **1** from 35 – 3 K**.**

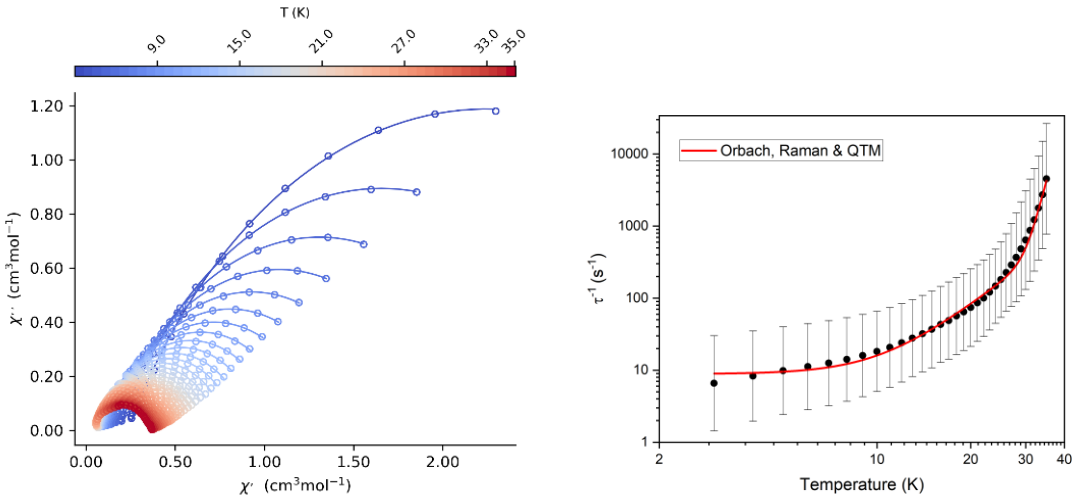

Figure S8 The Cole-Cole plot of in-phase (χ'_M) vs. out-of-phase (χ''_M) magnetic susceptibility in zero dc field (left) and plot of 1/relaxation time (τ^{-1}) *vs.* temperature for **1** in zero dc field. The red line represents the best fit to Orbach and Raman relaxation. Black vertical bars are estimated standard deviations in the relaxation times derived from Debye fits. U_{eff} = 625(1) K, τ_0 = 4.6(5) × 10^{-12} s, C = 2.9(13) x 10^{-4} K^{-n} s^{-1}, n = 3.4(1) and τ_{QTM}^{-1} = 0.113(8).

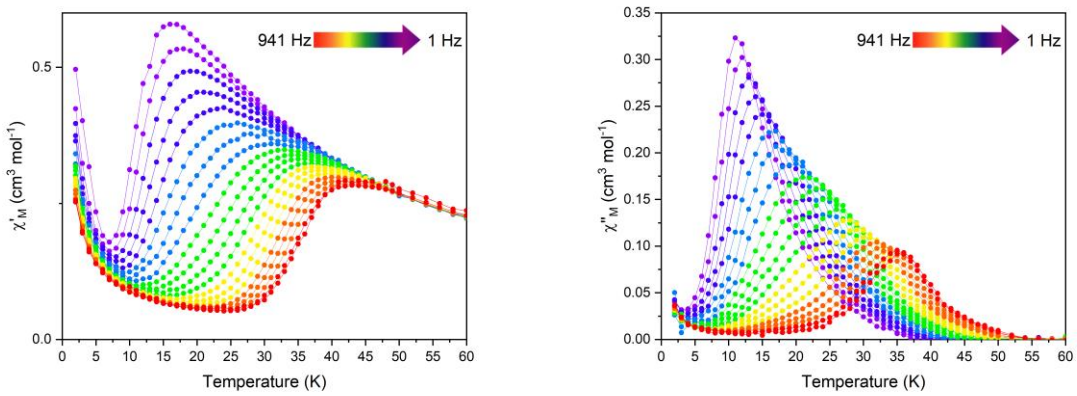

Figure S9 Temperature dependence of the in-phase (χ'_M) and out-of-phase (χ''_M) magnetic susceptibility in a 1000 Oe dc field for **1**.

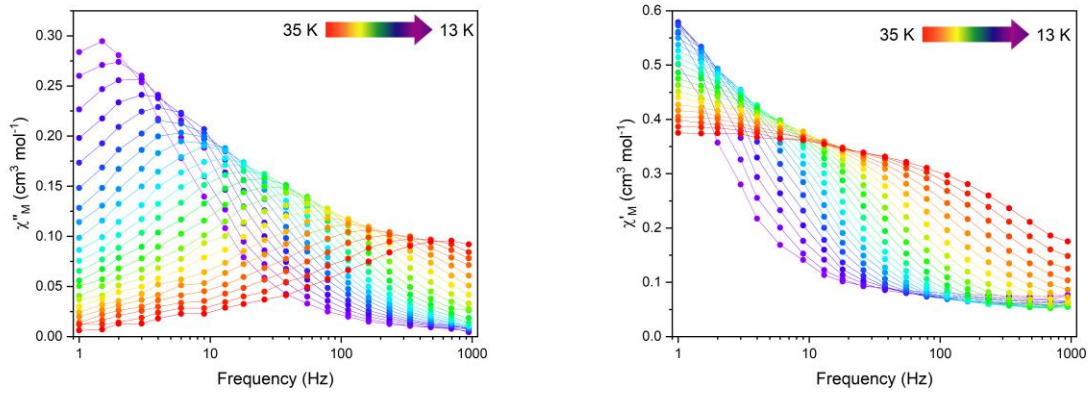

Figure S10 Frequency dependence of the in-phase (χ'_M) (left) and out-of-phase (χ''_M) (right) magnetic susceptibility in a 1000 Oe dc field for **1** from 35 – 13 K.

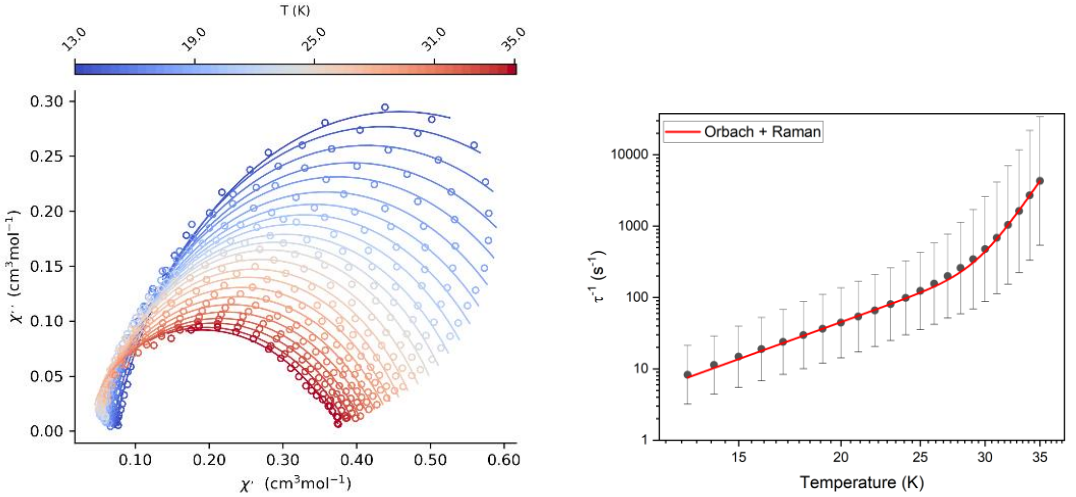

Figure S11 The Cole-Cole plot of in-phase (χ'_M) *vs*. out-of-phase (χ''_M) magnetic susceptibility in zero dc field (left) and plot of 1/relaxation time (τ^{-1}) vs temperature for **1** in a 1000 Oe dc field. The red line represents the best fit to Orbach and Raman relaxation. Black vertical bars are estimated standard deviations in the relaxation times derived from Debye fits. U_{eff} = 621(6) K, $\tau_0 = 5.0(8) \times 10^{-12}$ s, C = 1.80 x 10^{-4} K^{-n} s^{-1} (fixed) and n = 4.15 (fixed).

Table S3 A comparison of the magnetic properties of SIM-POM compounds reported in the literature, where the POM acts as an anion.

Compound / SIM	**Applied Field (Oe)**	**U_{eff} (K)**	**$T_{B(hyst)}$ (K)**	**POM unit**	**Role of the POM**	**Ref.**
$[Dy(H_2O)_5(Cy_3PO)_2][W_{12}PO_{40}]$	/	625	12 (200 Oe/s)	$[PW_{12}O_{40}]^{3-}$	**Anion**	This work
$[Dy(OPPh_3)_4(H_2O)_3][PMo_{12}O_{40}]$	/	/	/	$[PMo_{12}O_{40}]^{3-}$	**Anion**	S1
$[\{Ln\}\{Dy_4(\mu_3\text{-}OH)_4(H_2O)_{10}\}\{(\boldsymbol{m}\text{-}\mathbf{L_{Ru}})_4(HCOO)_2\}]\{SiW_{12}O_{40}\}_2\cdot x DMF\cdot y H_2O$	/	/	/	$[SiW_{12}O_{40}]^{3-}$	**Anion**	S2
$[Dy(bpyno)_4][PMo_{12}O_{40}]\cdot 2H_2O$	/	/	/	$[PMo_{12}O_{40}]^{3-}$	**Anion**	S3
$[Dy(OPPh_3)_4(H_2O)_3][PW_{12}O_{40}]\cdot 4H_2O$	2000	91	/	$[PW_{12}O_{40}]^{3-}$	**Anion**	S4

Table S4 A comparison of the magnetic properties of SIM-POM complexes and compounds reported in the literature, where the POM acts as a ligand.

Compound / SIM	**Applied Field (Oe)**	**U_{eff} (K)**	**$T_{B(hyst)}$ (K)**	**POM unit**	**Role of the POM**	**Ref.**
$[\{(AsW_9O_{33})_3Dy_2(H_2O)_4W_4O_9(H_2O)\}_2(NH_2(CH_2PO_3)_2)]^{33-}$	0	141	8 (500 Oe/s)	$[AsW_9O_{33}]^{9-}$	Ligand	S5
$[Dy_2(NMP)_{12}(PW_{12}O_{40})]$ $[PW_{12}O_{40}]$	1000	6.55	/	$[PW_{12}O_{40}]^{3-}$	Ligand	S6
$[Dy^{III}(Pc)(PW_{11}O_{39})]^{6-}$	500	47.5	/	$[PW_{11}O_{39}]^{7-}$	Ligand	S7
$[ErW_{10}O_{36}]^{9-}$	0	55.8	/	$[ErW_{10}O_{36}]^{9-}$	Ligand	S8
$[Dy_2(\mu\text{-}OH)_2(\gamma\text{-}SiW_{10}O_{36})_2]^{12-}$	0	65.7	/	$[\gamma\text{-}SiW_{10}O_{36}]^{8-}$	Ligand	S9
$(TBA)_{8.5}H_{1.5}[(PW_{W11}O_{39})_2Dy_2X_2(H_2O)_2]\cdot 6H_2O$ (X = OH (**a**), F (**b**))	0	98 (**a**) 74 (**b**)	2 (200 Oe/s) (**a**)	$[PW_{11}O_{39}]^{7-}$	Ligand	S10
$[\{Dy(OPPh_3)_3(H_2O)_3\}\{PW_{12}O_{40}\}]\cdot Ph_3PO\cdot H_2O$	0	310	/	$[PW_{12}O_{40}]^{3-}$	Ligand	S4

References

[S1] C. Hu, Y.-L. Lu, Y.-Z. Li, Y.-P. Yang, M. Liu, J.-M. Liu, Y.-Y. Li, Q.-H. Jin and Y.-Y. Niu, *Environ. Res.*, 2022, **206**, 112267.

[S2] L. Wang, W. Yang, F.-Y. Yi, H. Wang, Z. Xie, J. Tang and Z.-M. Sun, *Chem. Commun.*, 2013, **49**, 7911.

[S3] W. Zhou, X. Feng, H. Ke, Y. Li, J. Tang and E. Wang, *Inorg. Chim. Acta*, 2013, **394**, 770–775.

[S4] H. Kong, Z.-Y. Ruan, Y.-C. Chen, W. Deng, P.-Y. Liao, S.-G. Wu and M.-L. Tong, *Inorg. Chem.*, 2024, **63**, 15964–15972

[S5] Y. Huo, R. Wan, P. Ma, J. Liu, Y. Chen, D. Li, J. Niu, J. Wang and M.-L. Tong, *Inorg. Chem.*, 2017, **56**, 12687–12691.

[S6] J. Li, C. Yuan, L. Yang, M. Kong, J. Zhang, J.-Y. Ge, Y.-Q. Zhang and Y. Song, *Inorg. Chem.*, 2017, **56**, 7835–7841.

[S7] S. Sarwar, S. Sanz, J. van Leusen, G. S. Nichol, E. K. Brechin and P. Kögerler, *Dalton Trans.*, 2020, **49**, 16638–16642.

[S8] M. A. AlDamen, J. M. Clemente-Juan, E. Coronado, C. Martí-Gastaldo and A. Gaita-Ariño, *J. Am. Chem. Soc.*, 2008, **130**, 8874–8875.

[S9] K. Suzuki, R. Sato and N. Mizuno, *Chem. Sci.*, 2013, **4**, 596–600.

[S10] Y. Huo, Y.-C. Chen, S.-G. Wu, J.-L. Liu, J.-H. Jia, W.-B. Chen, B.-L. Wang, Y.-Q. Zhang and M.-L. Tong, *Inorg. Chem.*, 2018, **58**, 1301–1308.